AGU PUBLICATIONS

JGR

Journal of Geophysical Research: Oceans

RESEARCH ARTICLE

10.1002/2016JC012201

Seasonal warming of the Middle Atlantic Bight Cold Pool

S. J. Lentz[1]

[1]Physical Oceanography, Woods Hole Oceanographic Institution, Woods Hole, Massachusetts, USA

Key Points:
- The Cold Pool, a band of cold near-bottom water on the Middle Atlantic Bight continental shelf, warms gradually from spring to early fall
- The warming of the Cold Pool is primarily due to vertical mixing across the seasonal thermocline
- The Cold Pool warms more rapidly over Georges Bank than in the southern MAB due to stronger tidal mixing over Georges Bank

Correspondence to:
S. J. Lentz,
slentz@whoi.edu

Citation:
Lentz, S. J. (2017), Seasonal warming of the Middle Atlantic Bight Cold Pool, *J. Geophys. Res. Oceans*, *122*, 941–954, doi:10.1002/2016JC012201.

Received 29 JUL 2016
Accepted 4 JAN 2017
Accepted article online 10 JAN 2017
Published online 2 FEB 2017

Abstract The Cold Pool is a 20–60 m thick band of cold, near-bottom water that persists from spring to fall over the midshelf and outer shelf of the Middle Atlantic Bight (MAB) and Southern Flank of Georges Bank. The Cold Pool is remnant winter water bounded above by the seasonal thermocline and offshore by warmer slope water. Historical temperature profiles are used to characterize the average annual evolution and spatial structure of the Cold Pool. The Cold Pool gradually warms from spring to summer at a rate of order 1°C month^{-1}. The warming rate is faster in shallower water where the Cold Pool is thinner, consistent with a vertical turbulent heat flux from the thermocline to the Cold Pool. The Cold Pool warming rate also varies along the shelf; it is larger over Georges Bank and smaller in the southern MAB. The mean turbulent diffusivities at the top of the Cold Pool, estimated from the spring to summer mean heat balance, are an order of magnitude larger over Georges Bank than in the southern MAB, consistent with much stronger tidal mixing over Georges Bank than in the southern MAB. The stronger tidal mixing causes the Cold Pool to warm more rapidly over Georges Bank and the eastern New England shelf than in the New York Bight or southern MAB. Consequently, the coldest Cold Pool water is located in the New York Bight from late spring to summer.

1. Introduction

The Cold Pool is a band of cold bottom water over the middle and outer shelf of the Middle Atlantic Bight, extending from the southern flank of Georges Bank to near Cape Hatteras, during spring to early fall (Figure 1) [*Bigelow*, 1915, 1933; *Ketchum and Corwin*, 1964; *Boicourt and Hacker* 1976; *Beardsley et al*., 1976; *Beardsley and Boicourt*, 1981; *Houghton et al*., 1982; *Bignami and Hopkins*, 2003]. The Cold Pool is a 20–60 m thick layer of relatively uniform near-bottom water bounded above and onshore by the seasonal thermocline [e.g., *Bigelow*, 1933] and offshore by the shelfbreak front that separates the cooler Cold Pool water from the warmer slope water [e.g., *Linder and Gawarkiewicz*, 1998; *Fratantoni and Pickart*, 2007] (e.g., Figure 2). Consequently, the Cold Pool emerges in spring with the development of the seasonal thermocline and disappears in early fall with the erosion of the seasonal thermocline [*Bigelow*, 1933; *Lentz et al*., 2003]. The Cold Pool is a key feature in the seasonal evolution of the MAB thermal structure and consequently a comprehensive understanding of the MAB physical environment must include the processes controlling the seasonal evolution and spatial structure of the Cold Pool. (In the following MAB refers to the Middle Atlantic Bight and the southern flank of Georges Bank.)

The Cold Pool plays a central role in structuring the MAB ecosystem. The Cold Pool is a reservoir of nutrients over the shelf during the spring and summer [e.g., *Falkowski et al*., 1983; *Walsh et al*., 1987; *Marra et al*., 1990; *Hales et al*., 2009b] that feeds phytoplankton productivity [*Malone et al*., 1983; *Flagg et al*., 1994]. The Cold Pool also impacts fish distributions and behavior in the MAB. For example, yellowtail flounder depend on the Cold Pool over the spring and summer months for spawning and nursery grounds [*Sullivan et al*., 2005]. Northern species like red hake use the MAB habitat associated with the Cold Pool during their summer migration [*Nye et al*., 2009]. There is also growing evidence of interannual to decadal shifts in both MAB fish distributions and community structures; associated in part with thermal habitat preference and systematic changes in temperature [e.g., *Weinberg*, 2005; *Lucey and Nye*, 2010; *Nye et al*., 2009].

The Cold Pool is evident in the earliest observations of subsurface water temperatures in the MAB [e.g., *Libbey*, 1889]. However, *Bigelow* [1915, 1933] provided the first comprehensive description of the MAB Cold Pool using an extensive set of hydrographic surveys he collected between 1913 and 1932. Bigelow noted that the Cold Pool appeared in May as remnant winter water capped by the developing seasonal thermocline, gradually warmed during the summer, and disappeared in the fall with the destruction of the seasonal

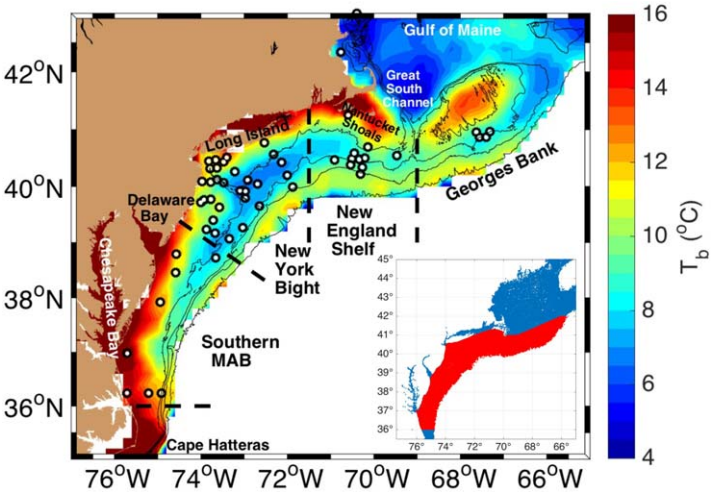

Figure 1. Mean near-bottom temperatures for July in the Middle Atlantic Bight and southern Gulf of Maine (the data set and processing are described in section 3). Temperature time series station locations (circles); boundaries between four subregions of the MAB (separated by dashed lines): the southern flank of Georges Bank, the New England Shelf, the New York Bight, and the Southern Middle Atlantic Bight; and the 50, 75, 100, and 1000 m isobaths (thin black lines) are shown. Inset shows entire region of compiled temperature profiles with the region encompassing the Cold Pool highlighted in red.

thermocline. Bigelow also noted that the coldest near-bottom water was consistently in the New York Bight during summer—"In each summer, again, the isotherms for the lowest values outlined a definite *cold pool*, centering in the offing of New York or a few miles further east, ..." *Ketchum and Corwin* [1964] argued that the gradual warming of the Cold Pool was due either to vertical mixing with warmer near-surface water or lateral mixing with warmer slope water. Based on limited salinity observations (1957–1959), they suggested that the relative importance of vertical and lateral mixing varied from year to year.

Direct current observations [e.g., *Beardsley et al*., 1976] and oxygen isotope ratio measurements [*Fairbanks*, 1982] subsequently emphasized the potential importance of along-shelf advection to the character and evolution of the Cold Pool. *Houghton et al*. [1982] provided a detailed examination of the evolution of the Cold Pool during the summer of 1979, taking advantage of an unusually large number of field programs in the MAB that year. They argued that either Nantucket Shoals or the southern New England shelf was the source of the coldest water in the Cold Pool. They also noted that the Cold Pool warmed at a rate of 0.04°C d^{-1} (~1°C $month^{-1}$) over the New England shelf in 1979, but did not determine the cause of the warming. *Houghton et al*. [1982] also showed there were substantial along-shelf variations in the temperature and structure of the Cold Pool in 1979, with the coldest water in the New York Bight, as noted previously by Bigelow. They surmised that the coldest water was in the New York Bight because this is the widest portion of the MAB continental shelf. Motivated by this supposition, *Ou and Houghton* [1982] used a simple model to suggest that the evolution of the Cold Pool temperature required along-shelf advection and that the presence of the coldest water in the New York Bight could be explained by an along-shelf variation in the heating rate that they attributed in part to variations in shelf width. Further evidence for the importance of along-shelf advection is provided by analysis of glider transects across the New Jersey shelf [*Castelao et al*., 2008, 2010]. *Castelao et al*. [2008] isolated a mode of variability (EOF 2 in their paper), associated with cooling of the Cold Pool that they concluded could only be explained by a 4–5 cm s^{-1} along-shelf advection of cold water from the north—consistent with *Houghton et al*. [1982] and *Beardsley et al*. [1985].

This study uses a comprehensive compilation of historical data to build on previous studies of the Cold Pool, notably *Bigelow* [1933] and *Houghton et al*. [1982], to address three objectives. The first objective is to develop a description of the average seasonal evolution and spatial structure of the Cold Pool. This provides a context for examining interannual variability and for determining whether the evolution of the Cold Pool in a given year, such as 1979, is typical or anomalous. The second objective is to determine the characteristics and cause of the gradual warming of the Cold Pool over the spring and summer. The third objective is to determine what controls the spatial and temporal evolution of the Cold Pool—particularly why the coldest water is observed in the New York Bight during the late spring and summer.

2. Data Sets and Processing

Historical temperature and salinity profiles from the National Oceanographic Data Center (NODC) World Ocean Atlas database [*Boyer et al*., 2013], the United Kingdom's Met Office Hadley Centre EN4 dataset (version EN4.1.1) [*Good et al*., 2013] and the National Marine Fisheries Service archive [*Fratantoni et al*., 2015]

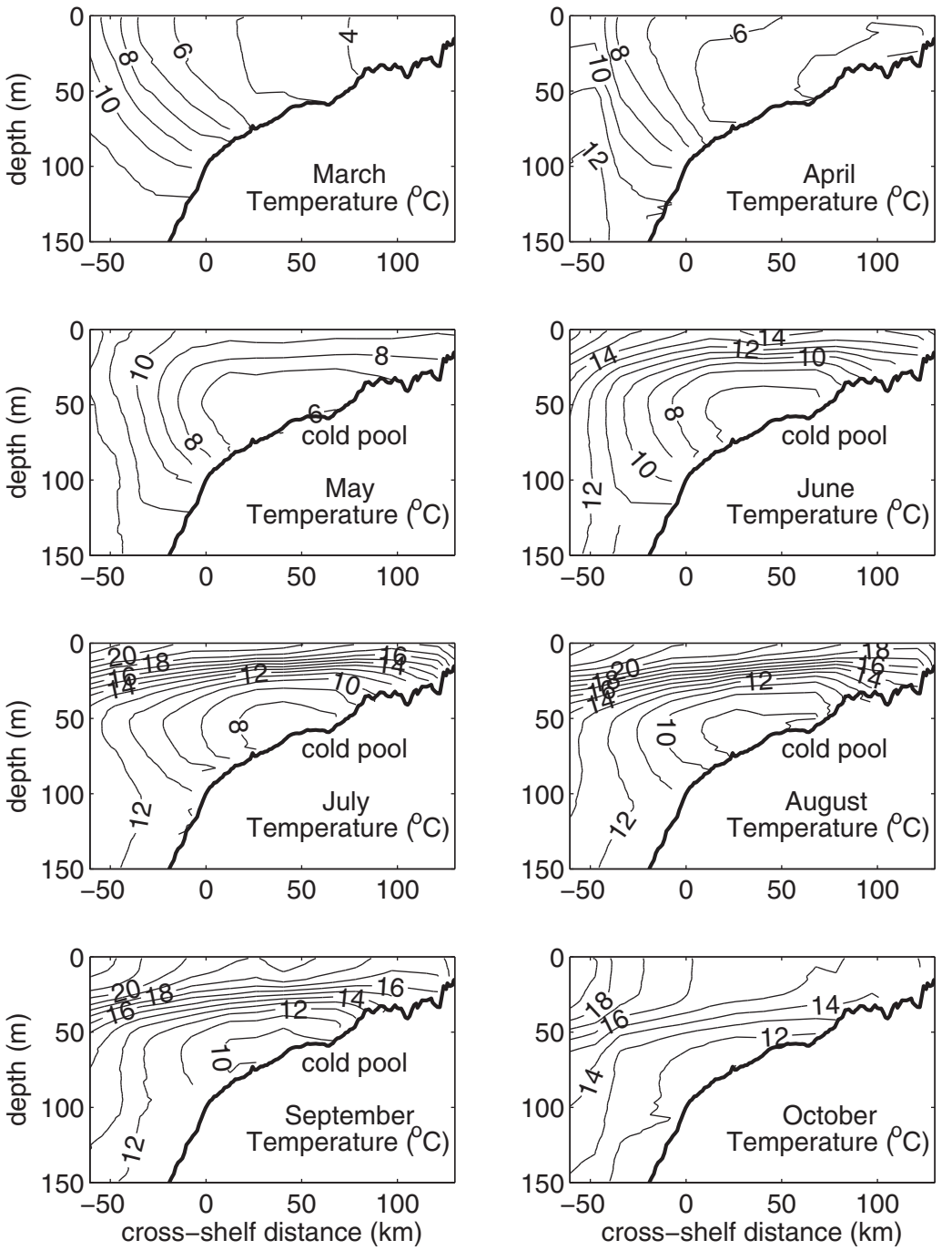

Figure 2. Average temperature sections across the New England Shelf for the months of March through October showing the Cold Pool bounded above by the seasonal thermocline and offshore by warmer slope water. Temperature contours are from profiles between 69°W and 73°W binned by water depth (10 m bins over the shelf and bounded by 150, 500, 1000, and 2000 m isobaths over the slope). Bathymetry is a characteristic transect across the New England shelf.

were collected for the Middle Atlantic Bight and Gulf of Maine. The water depth for each profile was determined from the latitude and longitude and high-resolution bathymetry for the MAB and Gulf of Maine (*NOAA National Centers for Environmental Information, U.S. Coastal Relief Model*, http://www.ngdc.noaa.gov/mgg/coastal/crm.html). Initial processing follows the procedures outlined in *Richaud et al.* [2016], including removing redundant profiles and obvious outliers (e.g., minimum water temperature in a profile greater than 30°C or less than −4°C) and averaging profiles that were taken less than 1 day apart and within 5 km

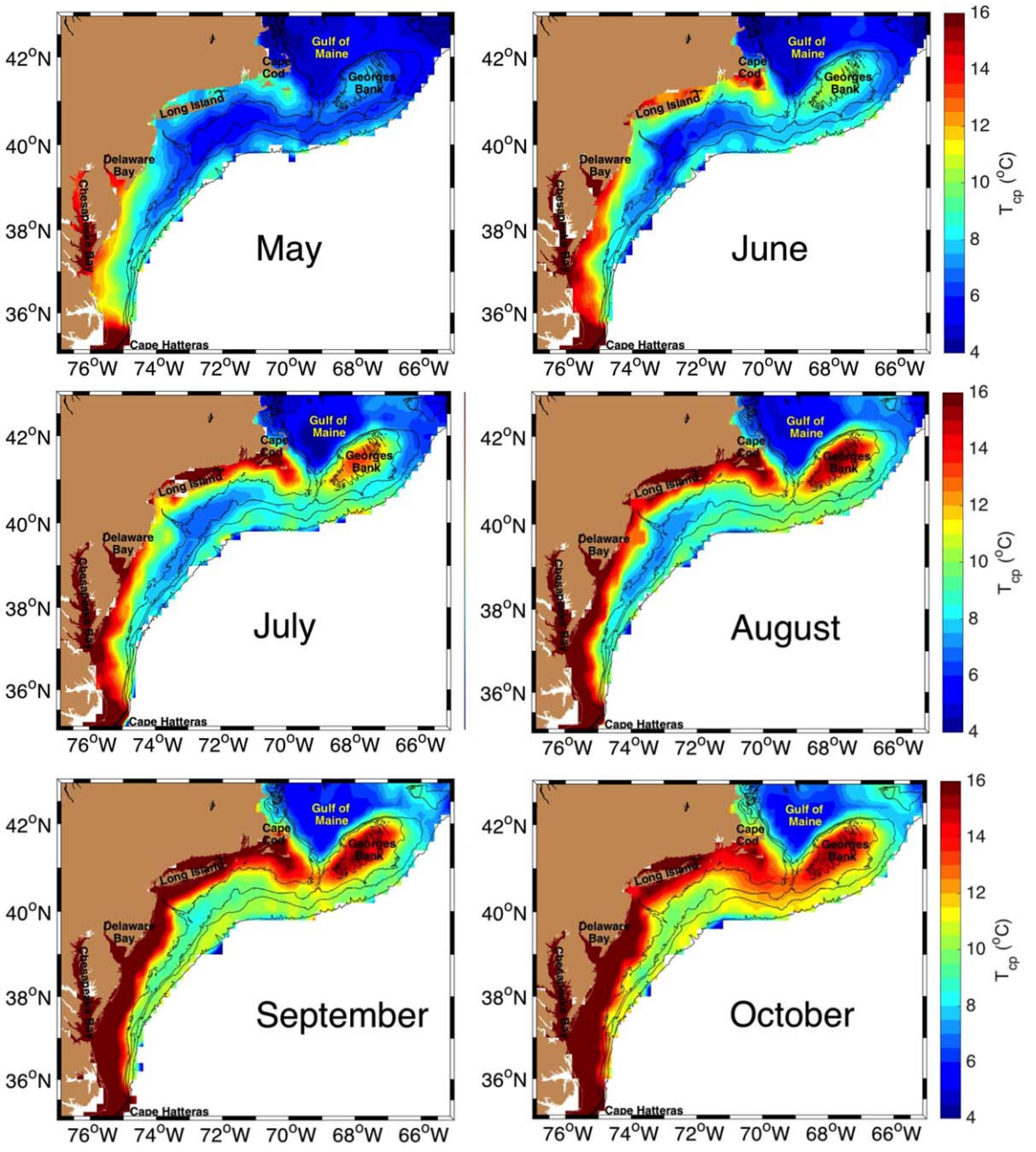

Figure 3. Monthly averaged Cold Pool temperatures (T_{cp}) in 0.4° × 0.4° latitude-longitude grid cells. In the region of the Cold Pool (inset Figure 1), standard errors of the monthly means are less than 0.2°C for more than 60% of the monthly averages and less than 0.4°C for over 90% of the monthly averages. Uncertainties are much larger over the slope and in the Gulf of Maine. The color scale was chosen to highlight the seasonal evolution of the spatial structure of the Cold Pool and consequently is often saturated in estuaries and over the inner shelf. The 50, 75, 100, and 1000 m isobaths are shown.

of each other. Only temperature profiles with a measurement within 20 m of the bottom were included. The choice of 20 m above the bottom was a compromise between ensuring that there was at least one temperature measurement within the Cold Pool and retaining as many profiles as possible.

The resulting data set includes 176,468 temperature profiles over the MAB and Gulf of Maine region, 35.5°N to 45°N, 65°W to 76°W, and water depths between 10 and 1000 m. While this broader data set was used to make maps of the Cold Pool temperature (e.g., Figure 3), all the subsequent analyses focus on a smaller region that encompasses the Cold Pool, between the 10 and the 1000 m isobaths and from 36°N to the northeastern edge of Georges Bank (Figure 1, red region inset). In this region encompassing the Cold Pool

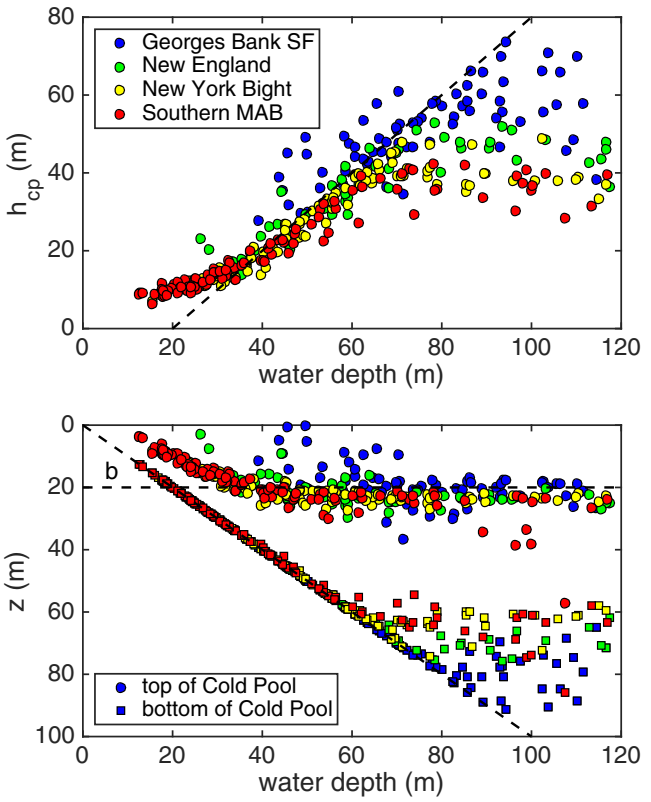

Figure 4. Dependence on water depth of average (1 April to 1 September) (a) Cold Pool thickness h_{cp} and (b) depth of the top and bottom of the Cold Pool. Dashed line in Figure 4a is $h_{cp}=D-20$ m, where D is water depth. Symbol colors indicate different regions of MAB.

there are 97,401 temperature profiles and 34,976 salinity profiles. Most of the temperature profiles in this region were collected between 1955 and 2014 and there are 8000–10,000 temperature profiles per month between March and October when the Cold Pool is present (there are ~5000 profiles per month in December and January). The spatial distribution of temperature profiles is not uniform; there are notable concentrations of profiles over Georges Bank, along the Hudson Shelf valley (Oleander line) [*Flagg et al*., 2006], and at lightship stations [*Shearman and Lentz*, 2010].

The Cold Pool temperature T_{cp} is defined as the minimum temperature in each profile following *Houghton et al*. [1982] because the Cold Pool water can be detached from the bottom over the outer shelf [e.g., *Bigelow*, 1915] (see also section 3 and Figure 4). All of the analyses were repeated using near-bottom temperature to characterize the Cold Pool (e.g., Figure 1) and the results are nearly indistinguishable (compare Figures 1 and 3 July). Cold Pool salinities S_{cp} are defined as the salinity at the depth of the minimum temperature in each profile. Monthly averages of T_{cp} are estimated for 0.4° × 0.4° latitude-longitude grid cells (Figure 3). The grid cell spacing was chosen to obtain the finest spatial resolution possible while reducing the uncertainty in the mean temperatures enough to provide an accurate description of the evolution of the Cold Pool. In the region encompassing the Cold Pool there are typically 50–150 profiles in a grid cell each month and standard deviations of T_{cp} (or T_b) are typically 1–2°C. Consequently, standard errors of the monthly means are less than 0.2°C for more than 60% of the monthly averages and less than 0.4°C for over 90% of the monthly averages. There are relatively few observations over the continental slope and consequently uncertainties in average temperatures are much greater over the slope. For some analyses the MAB was divided into four subregions: the Southern Flank of Georges Bank, the New England shelf, the New York Bight, and the southern MAB (Figure 1).

To complement the historical temperature profiles from ships and planes, moored temperature, salinity, and current profile time series from various field programs are also examined (Figure 1, circles) [*Lentz*, 2010]. The time series include: the 1955–1972 archive of daily temperature profiles collected at nine lightships in relatively shallow water (~30 m; except Nantucket Lightship 60 m) [*Shearman and Lentz*, 2010]; George Bank [*Butman et al*. 1987; *Brink et al*., 2009]; the New England shelf [*Beardsley et al*., 1985; *Aikman et al*., 1988; *Shearman and Lentz*, 2003], the New York Bight [*Mayer*, 1982], and the southern MAB [*Berger et al*., 1995; *Biscaye et al*., 1994; *Pietrafesa et al*., 2002]. The time series are at least 200 days long, and in some cases span several years.

3. Average Seasonal Evolution of the Cold Pool

Monthly averaged cross-shelf temperature sections from the New England shelf show the seasonal evolution of the Cold Pool (Figure 2). The Cold Pool is bounded offshore by slope water that exceeds 10°C

throughout the year and consequently is always warmer than the near-bottom shelf water. The Cold Pool begins to emerge in April, as decreasing storm activity and increasing surface heat flux lead to the development of the seasonal thermocline [e.g., *Lentz et al*., 2010]. The thermocline strengthens from May to August. By August the temperature difference between the surface and the Cold Pool reaches 10°C. The minimum temperature in the Cold Pool increases steadily from April to September at a rate of 1°C month^{-1} over the New England shelf. The Cold Pool disappears in fall (October–November) as vertical mixing from increasing storm activity and decreasing surface heat flux destroys the seasonal thermocline [*Lentz et al*., 2010].

The Cold Pool is first clearly evident throughout the MAB in May, when minimum temperatures at mid shelf are 6°C from the southern flank of Georges Bank to offshore of Delaware Bay and increase to about 8°C between Delaware Bay and Chesapeake Bay (Figure 3). In June, Cold Pool temperatures on the southern flank of Georges Bank and south of Nantucket Shoals have increased to about 9°C, while Cold Pool temperatures in the New York Bight and farther south have not changed. Consequently, the coldest water is in the New York Bight in June. Subsequently, from July to October, there is relatively rapid warming over Georges Bank and south of Nantucket Shoals and more gradual warming in the New York Bight and southern MAB. Consequently, the spatial pattern seen in June persists through October, with the coldest water centered in the New York Bight between Nantucket Shoals and Delaware Bay consistent with previous observations [e.g., *Bigelow*, 1915, 1933; *Houghton et al*., 1982].

The mean Cold Pool thickness h_{cp} from 1 April to 1 September for each longitude-latitude grid cell is defined as the vertical extent over which the mean temperature profile is within 1°C of the minimum temperature. The estimates of h_{cp} are similar if 0.5°C or 2°C are used because temperatures within the Cold Pool tend to be vertically uniform [*Bigelow*, 1933]. The bottom of the Cold Pool is located at the sea floor except near the shelfbreak, where the Cold Pool detaches from the bottom, riding over warmer but denser slope water (Figure 4b, squares). Offshore of the shelfbreak, the bottom of the Cold Pool is at ~60 m in the New York Bight and southern MAB, ~70 m off the New England shelf, and 80–90 m offshore of Georges Bank. The top of the Cold Pool is generally at ~20 m depth (Figure 4b, circles), except in water depths of less than 30 m where the thermocline intersects the bottom so there is not a well-defined Cold Pool. Outliers, where the estimated top of the Cold Pool is less than 20 m below the surface, correspond to tidally well-mixed regions over Georges Bank and Nantucket Shoals on the New England shelf. Consequently, the thickness of the Cold Pool is typically 20 m less than the water depth with a maximum thickness near the shelfbreak and over the slope of ~40 m in the New York Bight and southern MAB, ~50 m off the New England shelf, and 60–70 m offshore of Georges Bank (Figure 4a).

4. Warming of the Cold Pool

The warming of the Cold Pool seen in Figures 2 and 3 is a consistent feature from year to year. For example, time series of near-bottom temperature from the Nantucket Lightship (1955–1972) and two other moorings on the New England Shelf all exhibit a steady increase of ~0.04°C d^{-1} (~1°C month^{-1}) from mid-March to October (Figure 5). However, there is evidence of interannual variability in the duration of the Cold Pool. cold pool. In 1979 (Figure 5, blue trace), the year studied by *Houghton et al*. [1982], the steady warming persisted until the end of October when the near-bottom shelf water suddenly warmed abruptly from 12 to 16°C due to the onshore movement of warmer slope water [*Wright*, 1983]. In 1996, the Cold Pool and associated steady warming ended abruptly on 6 September (Figure 5, red trace) when Hurricane Edouard resulted in vertical mixing throughout the water column [*Dickey et al*., 1998; *Williams et al*., 2001; *Lentz et al*., 2003].

To determine the spatial distribution of the average Cold Pool warming rate, a linear regression analysis of the form $T_{cp}=at+b$, for the time t between 1 April and 1 September, is applied to the cold pool temperatures from the gridded historical temperature profiles (0.4° × 0.4° latitude-longitude grid cells) and near-bottom temperatures from the station time series. The estimated warming rates a exhibit two consistent spatial patterns (Figure 6). The warming rates increase as the water depth, or Cold Pool thickness, decreases and the warming rates are largest over the southern flank of Georges Bank and decrease along-shelf toward the southern MAB. For example, over the southern flank of Georges Bank warming rates increase from 0.03°C d^{-1} over the outer shelf $D \sim 100$ m ($h_{cp} \approx 80$ m) to 0.07°C d^{-1} in shallower water $D \sim 50$ m ($h_{cp} \approx 30$ m). Over the shallower southern MAB shelf warming rates are ~0.01°C d^{-1} for $D > 50$ m ($h_{cp} > 30$ m) and only reach 0.02°C d^{-1} for $D \approx 40$ m ($h_{cp} \sim 20$ m).

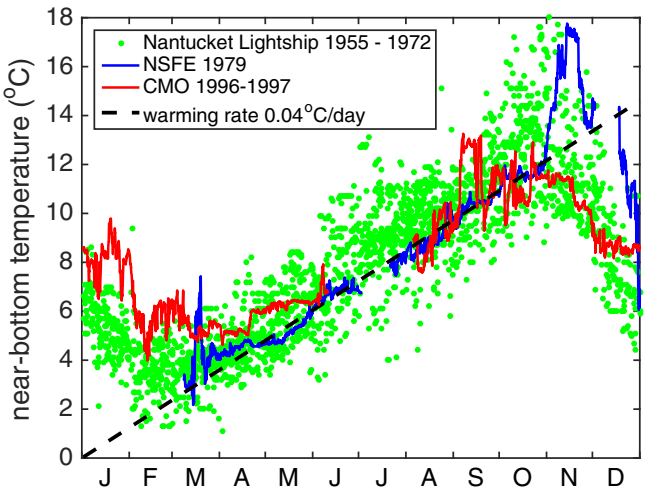

Figure 5. Daily near-bottom temperatures in ~65 m water depth on the New England shelf from the Nantucket Lightship and from moorings deployed during the 1979 Nantucket Shoals Flux Experiment and the 1996–1997 Coastal Mixing and Optics Study. A warming rate of 0.04°C d^{-1} is indicated. Note the abrupt temperature increases that mark the destruction of the seasonal thermocline and disappearance of the Cold Pool in early September 1996 (red) and late October 1979 (blue).

5. Mean Heat Balance

To interpret the observed warming rates it is useful to consider a simplified heat balance for the Cold Pool

$$\frac{\partial T}{\partial t}+v\frac{\partial T}{\partial y}=\frac{\partial}{\partial z}\left(K_z\frac{\partial T}{\partial z}\right)+\frac{\partial}{\partial x}\left(K_x\frac{\partial T}{\partial x}\right) \quad (1)$$

where x, y, z are the cross-shelf, along-shelf, and vertical coordinates, v is the along-shelf current, K_z is a vertical turbulent diffusivity, and K_x is a cross-shelf eddy diffusivity. In (1), the observed warming rate is related to along-shelf advection, vertical mixing and lateral exchange. Equation (1) assumes cross-shelf and vertical secondary circulations that may homogenize or displace the Cold Pool do not make a significant contribution to the heat balance. Along-shelf eddy diffusion that is likely to be small, and penetrating solar radiation (discussed below) are also assumed to be small. While along-shelf advection is significant (section 5.2), it cannot account for the consistent warming of the Cold Pool given the persistent along-isobath southwestward mean flow [*Lentz*, 2008] and the along-isobath variations in Cold Pool temperatures (Figure 3). This suggests that the warming is due either to vertical mixing of warmer thermocline water and/or lateral (and vertical) mixing of warmer slope water into the Cold Pool, as noted by *Ketchum and Corwin* [1964].

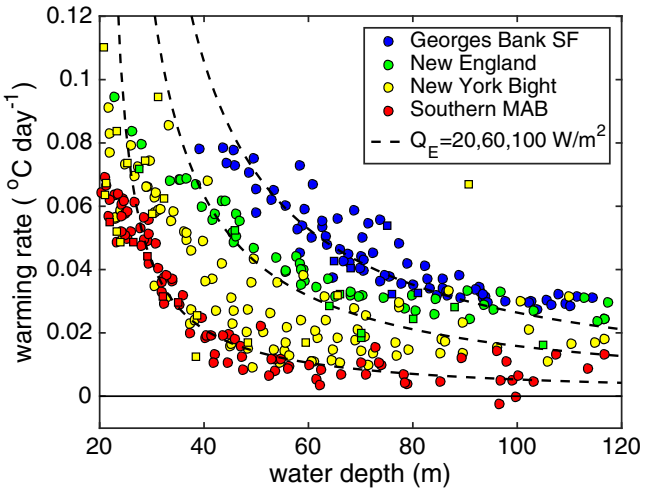

Figure 6. Dependence of estimated warming rate (1 April to 1 September) of T_{cp} on water depth, colors indicate different regions of MAB. Circles are estimates from gridded temperature profiles and squares are from individual moorings. The dashed lines indicate predicted dependence of warming rate on water depth assuming constant vertical heat fluxes from the thermocline into the Cold Pool and the Cold Pool thickness equals the water depth minus a 20 m thick thermocline (see Figure 4a). Confidence intervals (95%) on warming rates are generally less than 0.005°C d^{-1} and always less than 0.012°C d^{-1}.

5.1. Vertical or Lateral Mixing

The increase in the warming rate toward the coast (Figure 6), i.e., with distance away from the warmer slope water, suggests warming of the Cold Pool is primarily due to vertical mixing. Furthermore, the warming rate dependence on water depth is also consistent with a vertical flux of heat from the thermocline into the Cold Pool that is uniform across, but not along, the shelf. Assuming warming of the Cold Pool is only due to vertical mixing (no advection or lateral mixing) and integrating (1) from the sea floor (no heat flux) to the top of the Cold Pool yields

$$h_{cp}\frac{\partial T_{cp}}{\partial t}=K_z\frac{\partial T}{\partial z}\Big|_{z=h_{cp}}=\frac{Q_E}{\rho C_P}$$
$$\rightarrow \frac{\partial T_{cp}}{\partial t}=\frac{Q_E}{\rho C_P h_{cp}} \quad (2)$$

where Q_E is the downward heat flux at the top of the Cold Pool, $C_P \approx 3990$ Ws (kg °C)$^{-1}$ is the heat capacity of

seawater, $\rho \approx 1025$ kg m^{-3} is the density of seawater, and the temperature is assumed to be vertically uniform within the Cold Pool. The dependence of warming rate on Cold Pool thickness is consistent with (2) (black dashed lines in Figure 6) with larger heat fluxes through the thermocline Q_E over Georges Bank ($\sim$100 W m^{-2}) and the New England shelf than in the New York Bight and southern MAB ($\sim$30 W m^{-2}). The inferred heat flux through the thermocline over Georges Bank and the New England shelf is a substantial fraction of the net surface heat flux through the sea surface which ranges from 100 W m^{-2} in spring to a maximum of 200 W m^{-2} in July and August [*Beardsley et al*., 2003; *Lentz et al*., 2010; *Lentz*, 2010; *Fewings and Lentz*, 2011; *Georgas et al*., 2016]. The inferred heat flux through the thermocline in the southern half of the MAB is a smaller fraction of the net surface heat flux.

The direct heat flux into the Cold Pool due to penetrating solar radiation is order a few W m^{-2} using a mean summer surface heat flux for the New England shelf of 140 W m^{-2} [*Fewings and Lentz*, 2011] and assuming the 1% light level is at 30–40 m [e.g., *Hales et al*., 2009a; *Sosik et al*., 2001; *Chen et al*., 2003; *Chang and Dickey*, 2004] consistent with standard coastal water type models [*Simpson and Dickey*, 1981] and a climatology [*Ohlmann et al*., 1996]. This suggests penetrating solar radiation is too small by an order of magnitude or more to account for the observed warming of the Cold Pool.

Salinity variations may also indicate the relative importance of vertical mixing at the thermocline versus lateral mixing of slope water [*Ketchum and Corwin*, 1964]. Near-surface water tends to be slightly fresher than the Cold Pool while slope water is saltier, implying that vertical mixing of thermocline water would decrease the salinity of the Cold Pool, while lateral mixing of slope water would increase the salinity of the Cold Pool. However, a linear regression analysis to determine the salting rate of the Cold Pool $S_{cp}=ct+d$ (1 April to 1 September) is only suggestive because correlations with year day were low (magnitudes less than 0.4) and consequently estimates of salting rates are generally not significantly different from zero. Nevertheless, there is a consistent pattern (not shown)—salting rates are slightly negative on average (-0.005 psu d^{-1}) over most of the shelf suggesting thermocline mixing. However, near the shelfbreak salting rates are slightly positive on average (0.005 psu d^{-1}) suggesting mixing of slope water into the Cold Pool.

5.2. Along-Isobath Advection

To determine whether along-isobath advection is a significant term in the mean heat balance, a mean along-isobath velocity of $v_{cp}=5$ cm s^{-1} was assumed throughout the MAB [*Lentz*, 2008; *Houghton et al*., 1982] and the mean along-isobath temperature gradient $(\partial T_{cp}/\partial y)$ was estimated from the historical hydrographic observations of T_{cp}. *Lentz* [2008] found that mean along-isobath currents in the lower third of the water column ranged from 3 to 8 cm s^{-1}. Use of an along-isobath mean current that increases with increasing water depth following *Lentz* [2008] did not change the qualitative results. Mean temperature gradients from 1 April to 1 September were estimated along the 20–100 m isobaths in 10 m increments with an along-isobath averaging scale of 20 km. The resulting along-isobath temperature gradients were then projected onto the same 0.4° $\times$ 0.4° latitude-longitude grid used to estimate warming rates.

Mean along-isobath advective heat flux $-v_{cp}\partial T_{cp}/\partial y$ is small relative to the mean warming rate along the southern flank of Georges Bank, positive (warming) $\sim$0.02°C d^{-1} over the New England shelf and near zero in the New York Bight (Figure 7). In the southern MAB, the advective heat flux is negative (cooling) and larger than the warming rate, increasing in magnitude toward the south to -0.1°C d^{-1}. This pattern reflects the spatial distribution of Cold Pool temperature (Figure 3) since the mean along-isobath velocity is assumed constant throughout the region. The Cold Pool temperatures are relatively constant along-isobath over the southern flank of Georges Bank, decrease from the New England shelf to the New York Bight and then increase along the southern MAB shelf.

5.3. Estimation of Vertical Diffusivity in Thermocline

A rough estimate of the mean vertical turbulent diffusivity K_z above the Cold Pool can be made by vertically integrating the mean heat balance (1) assuming lateral mixing is negligible

$$h_{cp}\left(\frac{\partial T_{cp}}{\partial t}+v_{cp}\frac{\partial T_{cp}}{\partial y}\right)\approx K_z\frac{\partial T}{\partial z}\bigg|_{z=h_{cp}} \rightarrow K_z \approx h_{cp}\left(\frac{\partial T_{cp}}{\partial t}+v_{cp}\frac{\partial T_{cp}}{\partial y}\right)\Big/\frac{\partial T}{\partial z}\bigg|_{z=h_{cp}} \quad (3)$$

The mean vertical temperature gradient was estimated as the maximum temperature difference over 4 m depth intervals from the mean temperature profile in each grid cell. The resulting estimates of mean K_z are

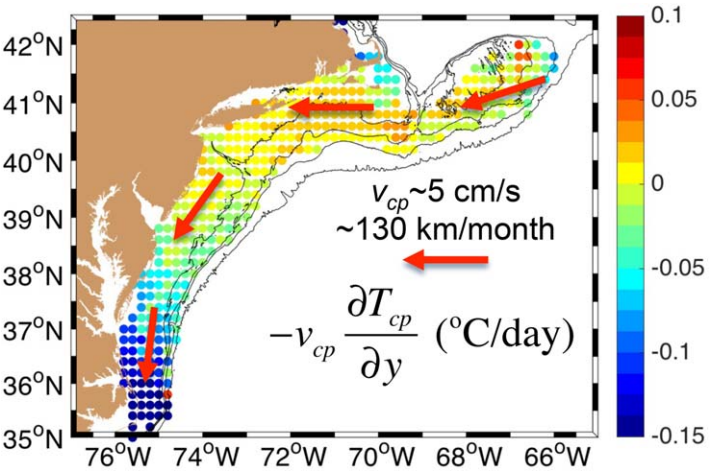

Figure 7. Average along-isobath heat flux (1 April to 1 September) based on a constant along-isobath southwestward current of 5 cm s^{-1} and the average along-isobath Cold Pool temperature gradients. Arrows indicate direction of along-isobath current and length of arrows corresponds to the along-isobath displacement (130 km) over a month.

based on a number of strong assumptions. Lateral or vertical flux of warmer slope water into the Cold Pool (last term equation (1)) is neglected so (3) will be inaccurate near the shelf-break. Since lateral mixing would tend to warm the Cold Pool the estimate of K_z is probably an upper bound. The estimate also neglects cross-shelf and vertical advection and is based on the mean heat budget over the spring summer, so, for example, it does not account for variations in thermal stratification on shorter time scales.

The mean vertical temperature gradient above the Cold Pool is relatively small over the southern flank of Georges Bank (0.1–0.2°C m^{-1}, Figure 8) and there is not a sharp thermocline (Figure 8, inset blue line). The vertical temperature gradient increases westward along the New England shelf and is relatively large in the New York Bight and southern MAB (0.5–0.8°C m^{-1}, Figure 8), where there is a sharp, clearly defined thermocline capping the Cold Pool (Figure 8, inset).

The mean thermal diffusivity estimated from (3) exhibits the opposite spatial pattern of the vertical temperature gradient. Estimated thermal diffusivities are at least an order of magnitude larger over the southern flank of Georges Bank (10^{-4} m^2 s^{-1}) than in the New York Bight or southern MAB (10^{-5} to 10^{-6} m^2 s^{-1}) (Figure 9). While clearly crude, the magnitudes and pattern of the estimated mean thermal diffusivities are in quantitative agreement with more direct estimates from tracer and microstructure measurements over Georges Bank [*Horne et al*., 1996; *Burgett et al*., 2001; *Houghton and Ho*, 2001; *Werner et al*., 2003; *Pease and Sundermeyer*, 2006], the New England shelf [*MacKinnon and Gregg*, 2003; *Oakey and Greenan*, 2004; *Ledwell et al*., 2004], and the southern MAB [*Wallace*, 1994].

The spatial distribution of the estimated thermal diffusivity (Figure 9) is consistent with the pattern of tidal currents and associated tidal mixing in the region [e.g., *Moody et al*., 1984; *Brown*, 1984; *He and Wilkin*, 2006; *Chen et al*., 2011]. There are relatively strong tidal currents and tidal mixing over the southern flank of Georges Bank and the eastern edge of the New England shelf because the Gulf of Maine is a resonant basin for the M_2 tide [*Garrett*, 1972]. In contrast, tidal currents and tidal mixing are relatively weak in the New York Bight and southern MAB [*Moody et al*., 1984; *Lentz et al*., 2001]. Consequently, the analyses presented here suggests that vigorous tidal mixing results in a large vertical heat flux over the southern flank of Georges Bank and the eastern New England shelf that warms the Cold Pool more

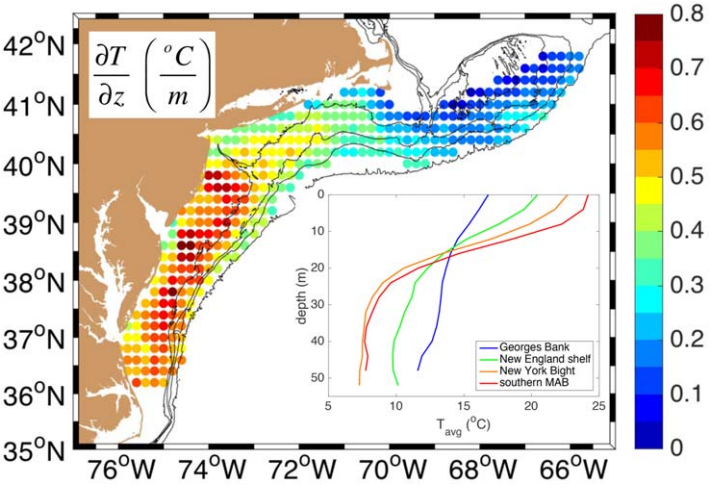

Figure 8. Maximum vertical temperature gradient (over 4 m intervals) in average (1 April to 1 September) temperature profiles for each latitude-longitude grid cell. Inset shows representative average temperature profiles in about 50 m water depth for the four regions denoted in Figure 1.

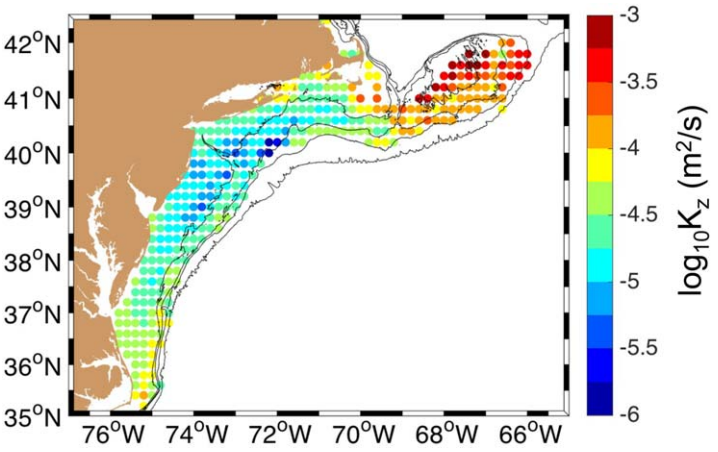

Figure 9. Log of the average (1 April to 1 September) thermal diffusivity in the thermocline above the Cold Pool estimated from equation (3).

rapidly than in the New York Bight or southern MAB where tidal mixing is weaker (Figure 6).

6. Spatial Pattern of Cold Pool Temperatures

The pattern of thermal diffusivities (Figure 9) provides a simple explanation for the spatial pattern in Cold Pool temperatures (Figure 3), specifically why the coldest water is consistently found in the New York Bight. Minimum shelf temperatures occur in March, and are about 5°C over Georges Bank and the New England shelf increasing to about 7°C in the southern MAB (Figure 10a). From April to October, Cold Pool temperatures along the 60 m isobath increase steadily over Georges Bank and the eastern New England shelf from 5°C in early April to 13°C by October (a rate of ~1°C month^{-1}) due to the strong tidal mixing of warm thermocline water into the Cold Pool. In contrast, Cold Pool temperatures in the New York Bight initially cool in early spring due to advection of colder water from the east and subsequently warm much less rapidly than Georges Bank because tidal mixing is relatively weak. In the southern MAB, there is very little change in Cold Pool temperatures until the fall breakdown of the thermocline because the relatively small heat flux from vertical mixing is largely balanced by the southward advection of colder water from the New York Bight. In summary, the coldest Cold Pool water is in the New York Bight because the water to the northeast (Georges Bank and eastern New England shelf) warms more rapidly due to tidal mixing and the water to the south (southern MAB) starts out and remains warmer.

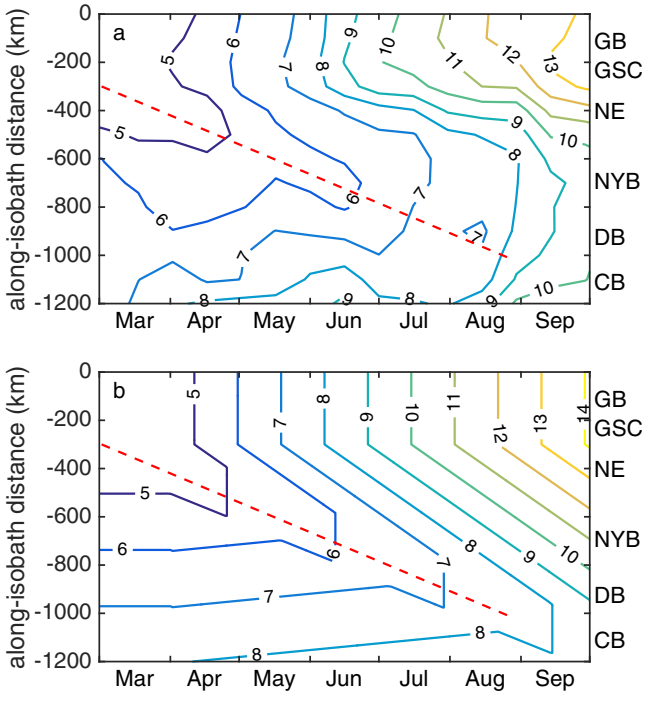

Figure 10. Contours of mean Cold Pool temperatures along the 60-m isobath as a function of time from March to September and along-isobath distance from the northeast corner of Georges Bank (0 km) to near Cape Hatteras (−1200 km) from (a) observations and (b) the simple model described in section 6 and Figure 11. Red dashed lines indicate an along-isobath displacement of 4 km d^{-1}. For reference the along-isobath locations of the center of the southern flank of Georges Bank (GB), Great South Channel (GSC), the New England shelf (NE), the apex of the New York Bight (New York Bight), the mouths of Delaware Bay (DB), and Chesapeake Bay (CB) are noted on right.

This conceptual picture is tested using the simplest model that incorporates the two key elements of the heat balance, along-shelf advection and a vertical heat flux into the Cold Pool that is larger over Georges Bank (including the eastern New England shelf) than the rest of the MAB (Figure 11). The assumed heat balance for the Cold Pool along the 60 m isobath (results are similar along 50 or 70 m isobaths)

$$\frac{\partial T_{cp}}{\partial t} + v_{cp}\frac{\partial T_{cp}}{\partial y} \approx \frac{Q_E}{\rho C_P h_{cp}} \qquad (4)$$

is integrated forward in time from April to September assuming a constant along-isobath velocity of v_{cp}=4 km

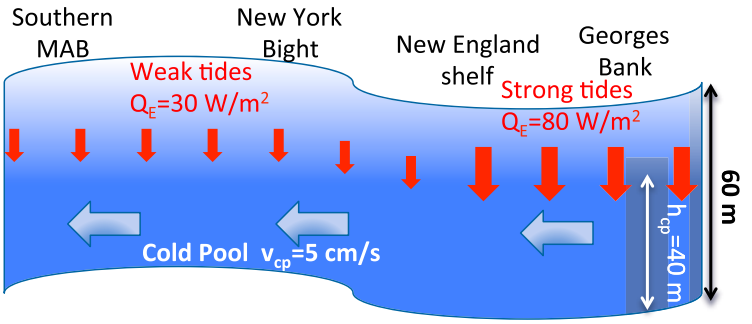

Figure 11. Schematic of elements in simple model of Cold Pool temperature evolution used in section 6 and Figure 10. Red arrows indicate the vertical flux of heat into the Cold Pool due to turbulent mixing and white arrows the constant along-isobath velocity of 4 km d^{-1}.

d^{-1} (~5 cm s^{-1}), a Cold Pool thickness of h_{cp}=40 m (Figure 4), ρ=1025 kg m^{-3}, and C_P=3990 Ws (kg °C)$^{-1}$. The Cold Pool temperature distribution along the 60 m isobath in March (Figure 10a) is used for the initial condition. At the upstream boundary, a one-dimensional balance is assumed, i.e., equation (4) with $\partial T_{cp}/\partial y$=0°C km^{-1}. The heat flux from the thermocline to the Cold Pool is assumed to be 100 W m^{-2} over the southern flank of Georges Bank and the eastern New England shelf and 40 W m^{-2} over the rest of the MAB (Figure 6). This is a simplified version of the model proposed by *Ou and Houghton* [1982] with no along-shelf variations in bathymetry (currents) and a different along-isobath distribution of heat flux through the thermocline.

This simple model reproduces the basic features of the observations, notably the tendency for the coldest Cold Pool water to be located in the vicinity of the New York Bight (compare Figures 10a and 10b). The agreement between the model and observations supports the basic hypothesis that the enhanced tidal mixing over Georges Bank has a substantial impact on the temporal evolution and spatial variations in Cold Pool temperatures. The model results also indicate that the observed tendency for the coldest water to be in the New York Bight region does not require along-shelf variations in the shelf width [*Houghton et al.*, 1982].

There are some notable differences between the model and the observations. Not surprisingly, the model does not reproduce the more rapid increase in Cold Pool temperatures in the New York Bight and southern MAB in late August and September, that are undoubtedly associated with the variable timing of the fall breakdown of stratification (e.g., Figure 5). Of more interest, there are stronger along-isobath temperature gradients in the vicinity of Great South Channel, between Georges Bank and the New England shelf, from June to September in the observations than in the model (Figure 10). Observed Cold Pool temperatures are also more uniform along-isobath than in the model in the New York Bight and southern MAB from June to September, suggestive of pooling of the Cold Pool water in the New York Bight [*Houghton et al.*, 1982; *Ou and Houghton*, 1982]. These discrepancies may be associated with the more complex circulation associated with Great South Channel that is not included in the simple model. Specifically, the flux of water from the Gulf of Maine to the New England shelf through Great South Channel [e.g., *Chen et al.*, 1995] and the associated recirculation that develops around Georges Bank in the summer [e.g., *Limeburner and Beardsley*, 1996; *Brink et al.*, 2003]. Another possibility is that these discrepancies are associated with the sudden broadening of the shelf west of Nantucket Shoals. Reducing the along-isobath velocity from 4 to 2 cm s^{-1} over the New England shelf in the model to crudely account for this broadening of the shelf results in both stronger gradients on the New England shelf and more uniform along-isobath Cold Pool temperatures in the New York Bight in closer agreement with the observations.

7. Implications for Nutrient Fluxes and Distributions

The along-shelf variations in the warming rates of the Cold Pool (Figure 6) and the inferred vertical mixing through the thermocline (Figure 9) have potential implications to nutrient fluxes into the euphotic zone. When the seasonal thermocline is present over the MAB shelf and southern flank of Georges Bank nutrient concentrations are consistently near zero above the thermocline due to rapid consumption in the euphotic zone while nutrient concentrations in the Cold Pool below the thermocline are substantially larger [e.g., *Walsh et al.*, 1987; *Falkowski et al.*, 1983; *Malone et al.*, 1983; *Mara et al.*, 1990; *Flagg et al.*, 1994; *Hales et al.*, 2009b]. The enhanced warming rates of the Cold Pool over Georges Bank due to tidal mixing implies there

should also be an enhanced upward vertical flux of nutrients [e.g., *Hales et al*., 2009a] from the Cold Pool into the euphotic zone presumably leading to enhanced productivity and reduced nutrient concentrations within the Cold Pool over Georges Bank relative to the New York Bight and southern MAB. While there are a complex set biological and physical processes influencing nutrient concentrations in the MAB [*Fennel et al*., 2006], it is intriguing that *Walsh et al*.'s [1987] observations that Cold Pool nutrient concentrations are lower over the southern flank of Georges Bank than in the New York Bight during the summer are qualitatively consistent with the upward nutrient flux distributions implied by the Cold Pool temperature budget. The characteristics of the nutrient concentrations and the relationship between upward vertical fluxes and primary production in the MAB are the subject of ongoing research.

8. Summary

Analysis of historical temperature profiles from the southern flank of Georges Bank and the Middle Atlantic Bight provides a description of the seasonal evolution of the Cold Pool that is consistent with previous descriptions by *Bigelow* [1933] primarily using surveys collected between 1927 and 1932 and by *Houghton et al*. [1982] for 1979. On average, the Cold Pool initially appears in April–May with the development of the seasonal thermocline over the shelf and persists through October when the seasonal thermocline is eroded by increasing storms and decreasing surface heat fluxes (Figures 2 and 3). The Cold Pool warms gradually through the spring and summer, but the warming rate is not spatially uniform. The warming rate is faster in shallower water, where the Cold Pool is thinner (Figure 6). The observed dependence on water depth is consistent with a vertical heat flux from the thermocline to the Cold Pool (Figure 6 dashed lines). The warming rate also decreases along-shelf from the northeast toward the southwest—that is, it is largest over Georges Bank and smallest in the southern MAB (Figure 6). The more rapid warming rate over Georges Bank relative to the rest of the MAB is likely due to enhanced vertical mixing associated with the much stronger tidal currents over Georges Bank (Figure 9). Though the coldest water is initially (March) over Georges Bank and the eastern New England shelf, from June to October the coldest Cold Pool water is located in the New York Bight (Figure 3). A simple model (Figure 11) indicates that the coldest Cold Pool water is located in the New York Bight because the water to the northeast (Georges Bank and eastern New England shelf) warms more rapidly due to tidal mixing and the water to the south (southern MAB) starts out and remains warmer (Figure 10).

Ideally this observational description of the seasonal evolution of the Cold Pool and the resulting conceptual model will motivate subsequent studies of the Cold Pool using more sophisticated numerical models of the region. The results of this study emphasize that to accurately reproduce the observed seasonal evolution of the Cold Pool numerical models must resolve the vertical structure of the thermocline and the vertical mixing across the thermocline. Numerical models could address two key limitations of this study: assuming a constant along-isobath current and an inability to quantify the contribution of lateral fluxes at the shelfbreak front to the seasonal evolution of the Cold Pool. A constant along-isobath current was assumed in the conceptual model of the Cold Pool because there are so few subsurface current observations. However, discrepancies between the conceptual model and the observations (Figure 10) suggest along-shelf variations in the mean circulation may influence the spatial structure and seasonal evolution of the Cold Pool. The analyses presented here suggest the steady warming of the Cold Pool is primarily due to vertical mixing across the thermocline, but seasonal changes in the Cold Pool salinities suggest, not surprisingly, that lateral fluxes are likely to be important near the shelfbreak.

Acknowledgments

Thanks to Wendell Brown of U. Mass. Dartmouth for reigniting my interest in the Cold Pool. Thanks also to two anonymous reviewers and Ken Brink (WHOI); their constructive suggestions substantially improved this paper. Data used in this study are available from the National Oceanographic Data Center (NODC) World Ocean Atlas database, the United Kingdom's Met Office Hadley Centre EN4 dataset (version EN4.1.1), and NOAA's Global Ocean Currents Database. Some hydrographic data used in this study were collected by the Oceans and Climate Branch of NOAA's Northeast Fisheries Science Center to advance understanding of the primary oceanographic influences on the ecology of the Northeast U.S. Shelf. Some moored time series are also available from the author (slentz@whoi.edu). This work was supported by NSF grant OCE-1332666.

References

Aikman, F., III, H. W. Ou, and R. W. Houghton (1988), Current variability across the New England continental shelf-break and slope, *Cont. Shelf Res.*, *8*, 625–651.

Beardsley, R. C., and W. C. Boicourt (1981), On estuarine and continental-shelf circulation in the Middle Atlantic Bight, in *Evolution of Physical Oceanography*, edited by B. A. Warren and C. Wunsch, pp. 198–233, MIT Press, Cambridge, Mass.

Beardsley, R. C., W. C. Boicourt, and D. V. Hansen (1976), Physical oceanography of the Middle Atlantic Bight, *The Middle Atlantic Continental Shelf and New York Bight*, vol. *2*, *Spec. Symp. Ser. [November 3–5, 1975]*, edited by G. Gross, pp. 20–34, Am. Soc. of Limnol. and Oceanogr., New York.

Beardsley, R. C., D. C. Chapman, K. H. Brink, S. R. Ramp, and R. Schlitz (1985), The Nantucket Shoals Flux Experiment (NSFE79). Part I: A basic description of the current and temperature variability, *J. Phys. Oceanogr.*, *15*, 713–748.

Beardsley, R. C., S. J. Lentz, R. A. Weller, R. Limeburner, J. D. Irish, and J. B. Edson (2003), Surface forcing on the southern flank of Georges Bank, February–August 1995, *J. Geophys. Res.*, *108*(C11), 8007, doi:10.1029/2002JC001359.

Berger, T. J., P. Hamilton, R. J. Wayland, J. O. BlantonW. C. Boicourt, J. H. Churchill, and D. R. Watts (1995), A physical oceanographic field program offshore North Carolina, Final Synthesis Report. OCS Study MMS 94-0047, U.S. Department of the Interior, Mineral Management Service, Gulf of Mexico OCS Region, 345 pp., New Orleans, La.

Bigelow, H. B. (1915), Exploration of the coast water between Nova Scotia and Chesapeake Bay, July and August, 1913, by the U. S. Fisheries Schooner Grampus, *Bull. Mus. Comp. Zool.*, *59*, 151–359.

Bigelow, H. B. (1933), Studies of the waters on the continental shelf, Cape Cod to Chesapeake Bay. 1: The cycle of temperature, *Pap. Phys. Oceanogr. Meteorol.*, *2*(4), 135 pp.

Bignami, F., and T. S. Hopkins (2003), Salt and heat trends in shelf waters of the southern Middle-Atlantic Bight, *Cont. Shelf Res.*, *23*, 647–667.

Biscaye, P. E., C. N. Flagg, and P. G. Falkowski (1994), The Shelf Edge Exchange Processes Experiment, SEEP-II: An introduction to hypotheses, results and conclusions, *Deep Sea Res., Part II*, *41*, 231–252.

Boicourt, W. C., and P. W. Hacker (1976), Circulation on the Atlantic continental shelf of the United States, Cape May to Cape Hatteras, in *Memoires de la Societe Royale des Sciences de Liege*, edited by J. C. J. Nihoul, pp. 187–200, Univ. of Liege, Liege, Belgium.

Boyer, T. P., et al. (2013), World Ocean Database 2013, Sydney Levitus, Ed.; Alexey Mishonov, Technical Ed., *NOAA Atlas NESDIS 72*, 209 pp., NOAA Print. Off., Silver Spring, Md.

Brink, K. H., R. Limeburner, and R. C. Beardsley (2003), Properties of flow and pressure over Georges Bank as observed with near-surface drifters, *J. Geophys. Res.*, *108*(C11), 8001, doi:10.1029/2001JC001019.

Brink, K. H., R. C. Beardsley, R. Limeburner, J. D. Irish, and M. Caruso (2009), Long-term moored array measurements of currents and hydrography over Georges Bank: 1994–1999, *Prog. Oceanogr.*, *82*(3), 191–223.

Brown, W. S. (1984), A comparison of Georges Bank, Gulf of Maine and New England Shelf tidal dynamics, *J. Phys. Oceanogr.*, *14*, 145–167, doi:10.1175/1520-0485(1984)014<0145:ACOGBG>2.0.CO;2.

Burgett, R. L., D. Hebert, and N. S. Oakey (2001), Vertical structure of turbulence on the southern flank of Georges Bank, *J. Geophys. Res.*, *106*, 22,545– 22,558.

Butman, B., J. W. Loder, and R. C. Beardsley, (1987), The seasonal mean circulation: Observation and theory, in *Georges Bank*, edited by R. H. Backus, pp. 125–138, MIT Press, Cambridge, Mass.

Castelao, R., S. Glenn, O. Schofield, R. Chant, J. Wilkin, and J. Kohut (2008), Seasonal evolution of hydrographic fields in the central Middle Atlantic Bight from glider observations, *Geophys Res. Lett.*, *35*, L03617, doi:10.1029/2007GL032335.

Castelao, R., S. M. Glenn, and O. Schofield (2010), Temperature, salinity and density variability in the central Middle Atlantic Bight, *J. Geophys. Res.*, *115*, C10005, doi:10.1029/2009JC006082.

Chang, G. C., and T. D. Dickey (2004), Coastal ocean optical influences on solar transmission and radiant heating rate, *J. Geophys. Res.*, *109*, C01020, doi:10.1029/2003JC001821.

Chen, C., R. C. Beardsley, and R. Limeburner (1995), Variability of currents in late spring in the northern Great South Channel, *Cont. Shelf Res.*, *15*, 451–573, doi:10.1016/0278-4343(94)00056-S.

Chen, C., R. Beardsley, P. Franks, and J. Van Keuren (2003), Influence of diurnal heating on stratification and residual circulation on Georges Bank. *J. Geophys. Res.*, *108*(C11), 8008, doi:10.1029/2001JC001245.

Chen, C., H. Huang, R. C. Beardsley, Q. Xu, R. Limeburner, G. W. Cowles, Y. Sun, J. Qi, and H. Lin (2011), Tidal dynamics in the Gulf of Maine and New England Shelf: An application of FVCOM, *J. Geophys. Res.*, *116*, C12010, doi:10.1029/2011JC007054.

Dickey, T. D., G. C. Chang, Y. C. Agrawal, A. J. Williams III, and P. S. Hill (1998), Sediment resuspension in the wakes of Hurricanes Edouard and Hortense, *Geophys. Res. Lett.*, *25*, 3533–3536.

Fairbanks, R. G. (1982), The origin of continental shelf and slope water in the New York Bight and Gulf of Maine: Evidence from $H_2^{18}O/H_2^{16}O$ ratio measurements, *J. Geophys. Res.*, *87*, 5796–5808.

Falkowski, P. G., J. Vidal, T. S Hopkins, G. T. Rowe, T. E. Whitledge, and W. G. Harrison (1983), Summer nutrient dynamics in the Middle Atlantic Bight: primary production and utilization of phytoplankton carbon, *J. Plankton Res.*, *5*, 515–537.

Fennel, K., J. Wilkin, J. Levin, J. Moisan, J. O'Reilly, and D. Haidvogel (2006), Nitrogen cycling in the Middle Atlantic Bight: Results from a three-dimensional model and implications for the North Atlantic nitrogen budget, *J. Geophys. Res.*, *111*, C06003, doi:10.1029/2005JC003116.

Fewings, M. R., and S. J. Lentz (2011), Summertime cooling of the shallow continental shelf, *J. Geophys. Res.*, *116*, C07015, doi:10.1029/2010JC006744.

Flagg, C. N., C. D. Wirick, and S. L. Smith (1994), The interaction of phytoplankton, zooplankton and currents from 15 months of continuous data in the Mid-Atlantic Bight, *Deep Sea Res., Part II*, *41*, 411–436.

Flagg, C. N., M. Dunn, D.-P. Wang, T. Rossby, and R. Benway (2006), A study of the currents of the outer shelf and upper slope from a decade of shipboard ADCP observations in the Middle Atlantic Bight, *J. Geophys. Res.*, *111*, C06003, doi:10.1029/2005JC003116.

Fratantoni, P. S., and R. S. Pickart (2007), The western North Atlantic shelfbreak current system in summer, *J. Phys. Oceanogr.*, *37*, 2509–2533, doi:10.1175/JPO3123.1.

Fratantoni, P. S., T. Holzworth-Davis, and M. H. Taylor (2015), Description of oceanographic conditions on the Northeast US Continental Shelf during 2014, *Northeast Fish Sci. Cent. Ref. Doc. 15-21*, 41 pp., U.S. Dep. Comm., Wood Hole, Mass., doi:10.7289/V5SQ8XD2.

Garrett, C. (1972), Tidal resonance in the Bay of Fundy and Gulf of Maine, *Nature*, *238*, 441–443, doi:10.1038/238441a0.

Georgas, N., L. Yin, Y. Jiang, Y. Wang, P. Howell, V. Saba, J. Schulte, P. Orton, and B. Wen (2016), An open-access, multi-decadal, three-dimensional, hydrodynamic hindcast dataset for the Long Island Sound and New York/New Jersey Harbor Estuaries, *J. Mar. Sci. Eng.*, *4*, 48.

Good, S. A., M. J. Martin, and N. A. Rayner (2013), EN4: Quality controlled ocean temperature and salinity profiles and monthly objective analyses with uncertainty estimates, *J. Geophys. Res. Oceans*, *118*, 6704–6716, doi:10.1002/2013JC009067.

Hales, B., D. Hebert, and J. Marra (2009a), Turbulent supply of nutrients to phytoplankton at the New England shelf break front, *J. Geophys. Res.*, *114*, C05010, doi:10.1029/2008JC005011.

Hales, B., R. D. Vaillancourt, L. Prieto, J. Marra, R. Houghton, and D. Hebert (2009b), High-resolution surveys of the biogeochemistry of the New England shelfbreak during summer, 2002, *J. Mar. Syst.*, *78*(3), 426–441, doi:10.1016/j.jmarsys.2008.11.024.

He, R., and J. L. Wilkin (2006), Barotropic tides on the southeast New England shelf: A view from a hybrid data assimilative modeling approach, *J. Geophys. Res.*, *111*, C08002, doi:10.1029/2005JC003254.

Horne, E. P., J. W. Loder, C. E. Naimie, and N. S. Oakey (1996), Turbulence dissipation rates and nitrate supply in the upper water column on Georges Bank, *Deep Sea Res., Part II*, *43*, 1683–1712.

Houghton, R. W., and C. Ho (2001), Diapycnal flow through the Georges Bank tidal front: A dye tracer study, *Geophys. Res. Lett.*, *28*, 33–36.

Houghton, R., R. Schlitz, R.C. Beardsley, B. Butman, and J. L. Chamberlin (1982), The Middle Atlantic Bight cold pool: Evolution of the temperature structure during summer 1979, *J. Phys. Oceanogr*, *12*, 1019–1029.

Ketchum, B. H., and N. Corwin (1964), The persistence of winter water on the continental shelf south of Long Island, New York, *Limnol. Oceangr.*, *9*, 467–475.
Ledwell, J. R., T. F. Duda, M. A. Sundermeyer, and H. E. Seim (2004), Mixing in a coastal environment. 1: A view from dye dispersion, *J. Geophy. Res.*, *109*, C10013, doi:10.1029/2003JC002194.
Lentz, S. J., M. Carr, and T. H. C. Herbers (2001), Barotropic tides on the North Carolina shelf, *J. Phys. Oceanogr.*, *31*, 1843–1859.
Lentz, S., K. Shearman, S. Anderson, A. Plueddemann, and J. Edson (2003), Evolution of stratification over the New England shelf during the Coastal Mixing and Optics study, August 1996-June1997, *J. Geophys. Res.*, *108*(C1), 3008, doi:10.1029/2001JC001121.
Lentz, S. J., R. K. Shearman, and A. J. Plueddemann (2010), Heat and salt balances over the New England continental shelf, August 1996 to June 1997, *J. Geophys. Res.*, *115*, C07017, doi:10.1029/2009JC006073.
Lentz, S. J. (2008), Observations and a model of the mean circulation over the Middle Atlantic Bight continental shelf, *J. Phys. Oceanogr.*, *38*, 1203–1221.
Lentz, S. J. (2010), The mean along-isobath heat and salt balances over the Middle Atlantic Bight continental shelf, *J. Phys. Oceanogr.*, *40*, 934–948.
Libbey, W. (1889), Report upon a physical investigation of the waters off the southern coast of New England, made during the summer of 1889 by the U. S. Fisheries Schooner Grampus, *Bull. U. S. Fish. Comm.*, *9*, 391–459.
Limeburner, R., and R. C. Beardsley (1996), Near-surface recirculation over Georges Bank, *Deep Sea Res., Part II*, *43*, 1547–1574.
Linder, C. A., and G. Gawarkiewicz (1998), A climatology of the shelfbreak front in the Middle Atlantic Bight, *J. Geophys. Res.*, *103*, 18,405–18,423.
Lucey, S. M., and J. A. Nye (2010), Shifting species assemblages in the Northeast US Continental Shelf Large Marine Ecosystem, *Mar. Ecol. Prog. Ser.*, *415*, 23–33.
MacKinnon, J., and M. Gregg (2003), Mixing on the late-summer New England shelf—Solibores, shear, and stratification, *J. Phys. Oceangr.*, *33*, 1476–1492.
Malone, T. C., T. S. Hopkins, P. G. Falkowski, and T. E. Whitledge (1983), Production and transport of phytoplankton biomass over the continental shelf of the New York Bight, *Cont. Shelf Res.*, *1*, 305–337.
Marra, J., R. W. Houghton, and C. Garside (1990), Phytoplankton growth at the shelf-break front in the Middle Atlantic Bight, *J. Mar. Res.*, *48*, 851–868.
Mayer, D. A. (1982), The structure of circulation: MESA physical oceanographic studies in New York Bight, 2, *J. Geophys. Res.*, 87, 9579–9588.
Moody, J. A., et al. (1984), Atlas of tidal elevation and cur- rent observations on the Northeast American continental shelf and slope, *U.S. Geol. Surv. Tech. Rep. Bull. 1611*, 122 pp., U.S. Geol. Surv., Alexandria, Va.
Nye, J. A., J. S. Link, J. A. Hare, and W. J. Overholtz (2009), Changing spatial distribution of fish stocks in relation to climate and population size on the Northeast United States continental shelf, *Mar. Ecol. Prog. Ser.*, *393*, 111–129, doi:10.3354/meps08220.
Oakey, N. S., and B. Greenan (2004), Mixing in a coastal environment, 2: A view from microstructure measurements, *J. Geophys. Res.*, C10014, doi:10.1029/2003JC002193.
Ohlmann, J. C., D. A. Siegel, and C. Gautier (1996), Ocean mixed layer radiant heating and solar penetration: A global analysis, *J. Clim.*, *9*, 2265–2280.
Ou, H. W., and R. Houghton (1982), A model of the summer progression of the cold-pool temperature in the Middle Atlantic Bight, *J. Phys. Oceanogr.*, *12*, 1030–1036.
Pease, C., and M. A. Sundermeyer (2006), Spatial and temporal variations of Richardson number on Georges Bank, *Geophy. Res. Lett.*, *33*, L06608, doi:10.1029/2005GL024903.
Pietrafesa, L. J., C. N. Flagg, L. Xie, G. L. Weatherly, and J. M. Morrison (2002), The winter/spring 1996 OMP current, meteorological, sea state and coastal sea level fields, *Deep Sea Res., Part II*, *49*, 4331–4354.
Richaud, B., Y.-O. Kwon, T. M. Joyce, P. S. Fratantoni, and S. J. Lentz (2016), Surface and bottom temperature and salinity climatology along the continental shelf off the Canadian and U.S. East Coasts, *Cont. Shelf Res.*, *124*, 165–181, doi:10.1016/j.csr.2016.06.005.
Shearman, R. K., and S. J. Lentz (2003), Dynamics of mean and subtidal flow on the New England shelf, *J. Geophys. Res.*, *108*(C8), 3281, doi: 10.1029/2002JC001417.
Shearman, R. K., and S. J. Lentz (2010), Long-term sea surface temperature variability along the U.S. east coast, *J. Phys. Oceanogr.*, *40*(5), 1004–1017.
Simpson, J. J., and T. D. Dickey (1981), The relationship between downward irradiance and upper ocean structure, *J. Phys. Oceanogr.*, *11*, 309–323.
Sosik, H. M., R. E. Green, W. S. Pegau, and C. S. Roesler (2001), Temporal and vertical variability in optical properties of New England shelf waters during late summer and spring, *J. Geophy. Res.*, *106*, 9455–9472.
Sullivan, M. C., R. K. Cowen, and B. P. Steves (2005), Evidence for atmosphere-ocean forcing of yellowtail flounder (*Limanda ferruginea*) recruitment in the Middle Atlantic Bight, *Fish. Oceanogr.*, *14*, 386–399.
Wallace, D. W. R. (1994), Anthropogenic chlorofluoromethanes and seasonal mixing rates in the Middle Atlantic Bight, *Deep Sea Res., Part II*, *41*, 207–324.
Walsh, J. J., T. E. Whitledge, J. E. O'Reilly, W. C. Phoel, and A. F. Draxler (1987), Nitrogen cycling on Georges Bank and the New York Shelf: A comparison between well-mixed and seasonally stratified waters, in *Georges Bank*, edited by R. H. Backus, pp. 234–246, MIT Press, Cambridge, Mass.
Weinberg, J. R. (2005), Bathymetric shift in the distribution of Atlantic surf clams: Response to warmer ocean temperature, *ICES J. Mar. Sci.*, *62*, 1444–1453.
Werner, S. R., R. C. Beardsley, S. J. Lentz, D. L. Hebert, and N. S. Oakey (2003), Observations and modeling of the tidal bottom boundary layer on the southern flank of Georges Bank, *J. Geophys. Res.*, *108*(C11), 8005, doi:10.1029/2001JC001271.
Williams, W. J., R. C. Beardsley, J. D. Irish, P. C. Smith, and R. Limeburner (2001), The response of Georges Bank to the passage of Hurricane Edouard, *Deep Sea Res., Part II*, *48*, 179–197.
Wright, W. R. (1983), Nantucket Shoals Flux Experiment Data Report I. Hydrography, NMFS, *NOAA Tech. Mem. NMFS-F/NEC-23*, 108 pp., Northeast Fish. Cent., Woods Hole, Mass.